Toxicology and Applied Pharmacology 329 (2017) 272–281

Contents lists available at ScienceDirect

Toxicology and Applied Pharmacology

journal homepage: www.elsevier.com/locate/taap

Invited Review Article

Antitumor effectiveness of a combined therapy with a new cucurbitacin B derivative and paclitaxel on a human lung cancer xenograft model

Lucas Lourenço Marostica [a], André Luís Branco de Barros [b], Juliana Oliveira [b], Breno Souza Salgado [c], Geovanni Dantas Cassali [d], Elaine Amaral Leite [b], Valbert Nascimento Cardoso [b], Karen Luise Lang [a], Miguel Soriano Balparda Caro [e], Fernando Javier Durán [f], Eloir Paulo Schenkel [a], Mônica Cristina de Oliveira [b], Cláudia Maria Oliveira Simões [a,*]

[a] Departamento de Ciências Farmacêuticas, Centro de Ciências da Saúde, Universidade Federal de Santa Catarina, Campus Trindade, CEP 88040-900 Florianópolis, Santa Catarina, Brazil
[b] Departamento de Produtos Farmacêuticos, Faculdade de Farmácia, Universidade Federal de Minas Gerais, Campus Pampulha, CEP 31270-901 Belo Horizonte, Minas Gerais, Brazil
[c] Departamento de Patologia, Centro de Ciências da Saúde, Universidade Federal do Espírito Santo, Campus Maruípe, CEP 29075-910 Vitória, Espírito Santo, Brazil
[d] Departamento de Patologia Geral, Instituto de Ciências Biológicas, Universidade Federal de Minas Gerais, Campus Pampulha, CEP 31270-901 Belo Horizonte, Minas Gerais, Brazil
[e] Departamento de Química, Centro de Ciências Físicas e Matemáticas, Universidade Federal de Santa Catarina, Campus Trindade, CEP 88040-900 Florianópolis, SC, Brazil
[f] UMYMFOR-CONICET, Departamento de Química Orgánica, Universidad de Buenos Aires, Buenos Aires, Argentina

ARTICLE INFO

Article history:
Received 18 March 2017
Revised 6 June 2017
Accepted 9 June 2017
Available online 10 June 2017

Keywords:
Cucurbitacins
Paclitaxel
Lung cancer
Xenograft lung tumor
Antitumor effect
Scintigraphic images

ABSTRACT

Non-small cell lung cancer (NSCLC) is one of the most common malignant tumors, with a high mortality rate due to the elevated risk of resistance. Natural cucurbitacins and their derivatives are recognized as promising antitumor compounds for several types of cancer, including NSCLC. In a recent study published by our research group, DACE (2-deoxy-2-amine-cucurbitacin E), which is a semisynthetic derivative of cucurbitacin B, showed potential *in vitro* synergistic antiproliferative effects combined with paclitaxel (PTX) in A549 cells. In sequence, the purpose of this study was to evaluate the *in vivo* antitumor efficacy of this combined therapy as well as with these drugs individually, using a human NSCLC xenograft model. Some indicators of sub chronic toxicity that could be affected by treatments were also assessed. The results obtained *in vivo* with the combined treatment (1 mg/kg + PTX 10 mg/kg) showed the most effective reduction of the relative tumor volume and the highest inhibition of tumor growth and proliferation, when compared with those of the single treatments. Furthermore, scintigraphic images, obtained before and after the treatments, showed that the most effective protocol able to reduce the residual viable tumor mass was the combined treatment. All treatment regimens were well tolerated without significant changes in body weight and no histological and functional damage to liver and kidney tissues. These results corroborate our previous *in vitro* synergistic effects published. Taken together, these insights are novel and highlight the therapeutic potential of DACE and PTX combination scheme for NSCLC.

Contents

Abbreviations: AST, aspartate aminotransferase; ALT, alanine aminotransferase; ATCC, American Type Culture Collection; CO_2, carbon dioxide; DAB, 3′3 diaminobenzidine; DACE, 2-deoxy-2-amine-cucurbitacin E; DMEM, Dulbecco's modified Eagle's medium; EGFR, epidermal growth factor receptor; FBS, fetal bovine serum; IPEN, Instituto de Pesquisas Energéticas e Nucleares; KeV, kiloelectronvolt; MBq, megabecquerel; NSCLC, non-small cell lung cancer; PBS, phosphate-buffered saline; P-gp, P-glycoprotein; PTX, paclitaxel; RTV, relative tumor volume; RVTM, residual viable tumor mass; TDA, total doses administered; TGI, tumor growth inhibition; TV, tumor volume; v:v, volume:volume ratio; w/v, weight/volume ratio; ^{99m}Tc-HYNIC-βAla-Bombesin$_{(7–14)}$, radionuclide technetium-99 m conjugated with bombesin.

* Corresponding author at: Laboratório de Virologia Aplicada, Departamento de Ciências Farmacêuticas, Centro de Ciências da Saúde, Universidade Federal de Santa Catarina (UFSC), Campus Universitário Trindade, Florianópolis 88040-900, SC, Brazil.
E-mail address: claudia.simoes@ufsc.br (C.M.O. Simões).

http://dx.doi.org/10.1016/j.taap.2017.06.007
0041-008X/

1. Introduction

Lung cancer remains is a main cause of cancer-related death worldwide. Among their different types, approximately 80% of case is classified as NSCLC. In addition to be considered an aggressive tumor, diagnosis is generally performed to late reduce the treatments effectiveness, in despite of the significant advances in understanding tumor progression and the discovery of new therapeutic options, such as epidermal growth factor receptor (EGFR) inhibitors and immunotherapy (Devarakonda et al., 2015; Ansari et al., 2016). In 2017, it was estimated that lung cancer will be the second cause of new diagnostics and cancer-related mortality (Siegel et al., 2017). NSCLC is a set of diseases showing genetic mutations and genomic heterogeneity, but even though most patients will initially respond to chemotherapy treatments, but they will likely develop resistance (Chen et al., 2014). These limitations highlight the requirements to search for new anticancer agents and/or combined therapies that can complement and/or improve the efficacy of the therapeutic alternatives currently available.

Several drugs used for cancer treatment are derived from natural products. Among all anticancer drugs discovered between 1940 and 2014, approximately 49% of the approved ones have been totally or partially derived from natural products (Newman and Cragg, 2016). Cucurbitacins are tetracyclic polyhydroxylated triterpenoids recognized as compounds with promising anticancer activity as it was demonstrated by *in vitro* and *in vivo* assays (Chen et al., 2005; Lee et al., 2010; Chen et al., 2012; Ríos et al., 2012; Alghasham, 2013; Arumuggam et al., 2015; Cai et al., 2015; Kaushik et al., 2015). Consequently, there is a growing concern in the research of new anticancer agents based on their strucutures, including semisynthetic derivatives. Recently, our research team described the potential cytotoxic effects of a cucurbitacin B derivative, named DACE, as well as other natural and semisynthetic cucurbitacins derivatives against different human cancer cell lines (Lang et al., 2011, 2012, 2014; Silva et al., 2013, 2015; Marostica et al., 2015). As previously described (Silva et al., 2015), DACE presents some advantages related to their physicochemical properties, when compared with the precursor cucurbitacin B. The semisynthesis process is simpler and might represent a new way to produce other anticancer compounds for additional studies. Furthermore, DACE was validated as a pharmacophore in a QSAR study published by our colleagues (Lang et al., 2014). Chemical modifications performed on DACE structure compared with its precursor also enable better biopharmaceutical properties as solubility and bioavailability (Silva et al., 2015).

Currently, drug combinations have been widely used and became the leading choice for treating many dreadful diseases, including cancer. The potential synergism achieved when chemotherapy drugs with different targets are combined represents a hopeful approach to improve the treatments of different types of cancer. The synergistic combinations can potentiate the therapeutic effectiveness and minimize problems, such as drug resistance, and still reduce the doses, and probably the toxicity (Chou, 2006; Li et al., 2014).

As cited above, our research group evaluated the antiproliferative effects *in vitro* of DACE combined with three different chemotherapy drugs (cisplatin, irinotecan and paclitaxel) on the human NSCLC cell line (A459). We showed that DACE combined with paclitaxel (PTX) at low concentrations presented promising synergistic antiproliferative effects, and was also less susceptible to drug resistance (Marostica et al., 2015).

The aim of the present study was to evaluate the antitumor effects of the same combined therapy with DACE and PTX with a xenograft model of human NSCLC to confirm *in vitro* synergistic effects previously detected. Furthermore, to check the effectiveness of the treatments scintigraphic images were used to calculate the reduction of residual viable tumor mass (RVTM). Histological and biochemical indicators of sub chronic toxicity induced by the tested treatments were also evaluated. Furthermore, cell proliferation of xenograft tumor after treatments was also investigated with an immunohistochemical protocol using the cancer cell proliferation biomarker Ki67.

2. Material and methods

2.1. Drugs and chemical reagents

DACE was synthesized from cucurbitacin B as previously described (Silva et al., 2015). PTX was supplied by Quiral Química (Juiz de Fora, MG, Brazil). Cremophor™, reagents and solvents for the radiolabeling procedures were purchased from Sigma-Aldrich (St. Louis, MO, USA). The peptide HYNIC-βAla-Bombesin$_{(7-14)}$ was obtained from GL Biochem (Minhang, SH, China). Technetium-99 m (^{99m}Tc) was acquired from a ^{99}Mo/^{99m}Tc generator supplied by *Instituto de Pesquisas Energéticas e Nucleares* (IPEN, São Paulo, SP, Brazil). Matrigel™ was obtained from Becton, Dickinson and Company (BD, Franklin Lakes, NJ, USA). Reagents for immunohistochemistry were purchased from NovoLink™ (Leica, Cambridge, UK) and monoclonal primary antibody (anti-ki67) used was obtained from Dako (Carpinteria, CA, USA).

2.2. Cell line

Human non-small-cell lung cancer cell line (A549) was obtained from ATCC® (CCL-185™) (Manassas, VA, EUA). Cells were cultured in Dulbecco's modified Eagle's medium (DMEM) from Gibco (Waltham, MA, USA) supplemented with 10% (v/v) fetal bovine serum (FBS) (Gibco), and 1% (v/v) of penicillin and streptomycin (Gibco). Cells were maintained in a humidified incubator with 5% CO_2 atmosphere at 37 °C and were routinely screened for the presence of potential contaminants, including mycoplasma.

2.3. Animals

Twenty-four female BALB/c nude mice (15–20 g) were purchased from IPEN. The experimental protocol was approved by the Committee on Care and Use of Experimental Animal Resources from the *Universidade Federal de Minas Gerais* (protocol number 118/2015) and follow the guide for the care and use of laboratory animals recommended by the Institute of Laboratory Animal Resources. Animals were kept under specific pathogen-free conditions in autoclaved cages with wood shavings, and free access to food and water. Temperature and relative humidity were controlled and a regulated light-dark cycle (12/12 h) was also applied.

2.4. Xenograft lung tumor model

A549 cells were cultured in DMEM supplemented with 10% FBS and 1% antibiotics. They were grown to confluence and then harvested by trypsin dissociation. After centrifugation (500 $\times g$ for 5 min), cells were resuspended (5×10^6 A549 cells) with Matrigel™: DMEM (1:1) and injected subcutaneously at the right lower flank (100 μl/animal). Tumors were allowed to grow for 30 days.

2.5. Treatments

After implantation and growth of tumors, the animals were randomly divided into four experimental groups containing six animals for each group. The control group was treated with the vehicle solution: Cremophor™/dehydrated ethanol 1:1 (v/v) solubilized in 0.9% saline solution (1:4, v/v). For the animals of the second group, DACE was administered at a dose of 1 mg/kg. The third group received PTX at a dose of 10 mg/kg. The fourth group received the combined treatment of DACE 1 mg/kg + PTX 10 mg/kg. The treatments were administered into the tail vein of lung tumor-bearing mice, twice a week, for three weeks. The first day of treatment administration was considered the day zero of this study. Treatments were started when the tumor volume in animals reached approximately 100 mm^3, thirty days after the inoculation of A549 tumor cells, and the endpoint of the experimental protocol was when the tumor volume of the control group animals reached approximately 500 mm^3, twenty-five days after starting treatments. In clinical practice, the administration route of PTX is intravenously, and consequently, treatments tested in this study were also administered by the intravenous route.

2.6. Antitumor activity

The evaluation of antitumor activity was based in tumor volume (TV) measurements calculated as follows: $TV = 0.52 \times (d1 \times d2^2)$, where d1 and d2 are the largest and the smallest perpendicular diameters, respectively, measured with a caliper MIP/E-103 (Mitutoyo, Suzano, SP, Brazil), as previously described (Roland et al., 2009). Tumor growth was monitored before of the treatment (day zero) and every two hours prior to the administration of each dose. Four days after the last administration, final tumor measurements were also performed (day 25). Alterations in TV were determined by considering the initial volume as 100% and calculating the percentages of increase or decrease, according to this initial volume. At the end of the experimental period, the relative tumor volume (RTV) for each experimental group was calculated as follows: (RTV = tumor volume on day 25/tumor volume on day 0). The percentage of tumor growth inhibition (TGI) was also calculated as follows: (TGI = (RTV from each treatment) × 100/RTV of control group).

2.7. Scintigraphic images

The radiolabeling of HYNIC-βAla-Bombesin$_{(7–14)}$ with ^{99m}Tc and the determination of the radiochemical purity were performed as previously described (De Barros et al., 2011). On days 0 and 25, the solution with 37 MBq ^{99m}Tc HYNIC-βAla-bombesin$_{(7–14)}$ was administered to BALB/c nude mice intravenously. Images were obtained after 4 h following administration of the radiolabeled complex. To obtain the images, mice were anesthetized with a mixture of ketamine (60 mg/kg) and xylazine (8 mg/kg) solution and placed in prone position under a gamma camera, model TH Nuclide TM22 (Mediso, Budapest, Hungary). A symmetric window of 20% was used for a peak energy of 140 KeV. The images (300.000 counts) were obtained and stored in an array 256 × 256. To quantify the uptake of the radiopharmaceutical ^{99m}Tc-HYNIC-βAla-Bombesin$_{(7–14)}$ by tumor focus, the images were analyzed by determining the target to non-target ratio as previously described (Diniz et al., 2008; De Barros et al., 2013). Initially, there was a design around the target area (tumor) and the non-target area (contralateral muscle). Then, the intensity of the radiation emitted was quantified in pixels for each one of the delineated areas and the target to non-target ratio was calculated as follows: (Target to non-target ratio = radiation of target area / radiation of non-target area). The results were expressed as the relative target to non-target ratio on day 25 (final) in comparison to the target to non-target ratio on day zero (initial), and calculated as follows: [Ratio = target to non-target ratio after treatments (day 25) / target to non-target ratio before of the treatments (day 0)].

2.8. Sub chronic toxicity analyses

Mice body weights were monitored on day zero, four days after each dose administered, and on day of euthanasia (day 25). Alterations in body weight during the experimental period were calculated in comparison with the initial weights. The evaluation of biochemical markers was performed for all animals at the end of the treatment protocol (day 25). Mice were anesthetized and blood samples were harvested at the brachial plexus with anticoagulant, and centrifuged to separate the serum. For the analyses of liver function, the levels of aspartate aminotransferase (AST), alanine aminotransferase (ALT) and alkaline phosphatase were determined. Nephrotoxicity was assessed by determining serum urea levels. Total protein and albumin levels were also quantified. All protocols were done according to the manufacturer's specifications (Bioclin Quibasa, Belo Horizonte, MG, Brazil), and the absorbances were measured in a microplate spectrophotometer (Benchmark Plus, Bio-Rad, Hercules, CA, USA).

2.9. Histological analyses

After treatments, animals were anesthetized and euthanized. Tumors, lung, femur, brain, heart, kidney, liver and spleen tissues were harvested and fixed in formalin (10% w/v in phosphate-buffered saline, PBS, pH 7.4). Tissue sections (4 μm-thick) were processed to light microscopy studies. Hematoxylin-eosin staining procedures were performed on paraffin-embedded sections prepared on glass slides. Histological sections of tumors were used for histopathological classification, and organs were used to search for toxicity. Images of histological sections were captured using a digital camera (Spot Insight Color; SPOT Imaging Solutions, Sterling Heights, MI, USA) attached to a microscope (Olympus BX-40; Olympus, Tokyo, Japan). SPOT® (version 3.4.5, Spot Software BV, Amsterdam, Netherlands) and Corel DRAW® (version 7.468, Corel Corporation, Ottawa, ON, Canada) software were used for image analyses.

2.10. Immunohistochemistry

Tissue sections (3 um-thick) of tumors were obtained and used for immunohistochemistry. Slides were incubated overnight with the

primary antibody (anti-Ki67 from mouse). The antigen-antibody reaction was detected using a polymeric labeling detection system (Advance HRP, Dako, Carpinteria, CA, USA), and 3′3-diaminobenzidine (DAB) was used as chromogen agent. Normal human skin was used as positive control. For negative control, mouse IgG antibody was used. Then, slides were counter-stained using Harris hematoxylin and subsequent evaluation by lighting microscopy. Ki67 staining was considered positive when cells revealed a dark brown nuclear staining. To calculate cell proliferation ratio, photomicrographs were obtained in five hotspots from each slide stained with anti-Ki67 antibody. Images were analyzed using the Immunoratio plugin in the NIH ImageJ software (version 1.44p, Rockville, MD, USA). Then, the percentages of cell proliferation were obtained.

2.11. Statistical analyses

Data were expressed as mean ± SE. To confirm the normality and homoscedasticity of variance, D'Agostino and Bartlett tests were applied, respectively. Variables without normal distribution were transformed by the equation: $y = \log(y + 100)$. The differences between the experimental groups were tested by analysis of variance (one-way ANOVA followed by Tukey's test). For statistical analyses, the 95% confidence interval was used, and the differences were considered statistically significant when $p < 0.05$. Data were evaluated with GraphPad Prism software (version 5.00, La Jolla, CA, USA).

3. Results and discussion

After 30 days, a xenograft lung tumor was successfully developed in all animals, and could be identified macroscopically. The average size of the tumors ranged from 100 to 300 mm^3. A previous histological analysis of this human lung cancer xenograft model performed by our group (Marostica et al., 2016) indicated that the mice developed a highly invasive growing tumor with markedly pleomorphic nuclei and increased nuclear-to-cytoplasmic ratio. The neoplastic cells were arranged in different patterns, including solid, acinar and lepidic mucinous variants. Besides, some tumors showed a mixed pattern similar to human lung adenocarcinomas of mixed type. Tumor stroma was scant and necrotic area of tumor tissue was a prominent feature consistently observed as well as apoptosis. Our study also showed that this xenograft model could be monitored with scintigraphic images by radiolabelling. It is important to comment that these histological characteristics are similar to those of NSCLC tumors observed in humans (Chen et al., 2014).

Table 1
Total doses administered (TDA), relative tumor volume (RTV) and tumor growth inhibition (TGI) of xenograft lung tumors after different treatments.

Treatment	TDA (mg/kg)	RTV	TGI (%)
Control group	–	1.81 ± 0.13	–
DACE 1 mg/kg	6 mg/kg	1.45 ± 0.16	20.9
PTX 10 mg/kg	60 mg/kg	1.33 ± 0.12	27.5
DACE 1 mg/Kg + PTX 10 mg/kg	DACE 6 mg/kg + PTX 60 mg/kg	0.75 ± 0.06[a,b,c]	59.5

TDA means the total dose administered for each animal for each experimental group, after treatments. RTV means the tumor volume ratio on final and initial time of the treatments. TGI means the tumor growth inhibition on final time for each treatment, and calculated as formula described on material and methods section. Data represent the mean ± SE ($n = 6$ animals/group). Symbols indicate differences statistically significant (one-way ANOVA followed by Tukey's test) with treatments compared.

[a] Represents differences statistically significant (p˜0.0001) when compared the combined treatment and control group.

[b] Represents differences statistically significant (p˜0.001) when compared the combined treatment and DACE alone.

[c] Represents differences statistically significant (p˜0.05) when compared the combined treatment and PTX alone.

As shown in Table 1, the combined treatment inhibited the tumor growth and was more effective to reduce the RTV when compared with the individual treatments and the control group. The tested doses were selected based on data from previous studies with DACE (Silva et al., 2015), PTX (Wall and Wani, 1995; Yamori et al., 1997; Huang et al., 2006; Milanovic et al., 2012) and cucurbitacin B (Iwanski et al., 2010; Kausar et al., 2013), which is a precursor of DACE, and all treatments included in these studies were well tolerated by the animals. Therefore, the doses tested in this study were selected based on the critical analysis of previous studies performed with the same lineage of animals evaluated in the present study, which demonstrated that these treatments and doses were well tolerated by BALB/c nude mice. The combined treatment regimen of DACE + PTX was selected for this *in vivo* xenograft model of NSCLC since their synergistic *in vitro* antiproliferative effects detected previously by our research team were the most effective against A549 cells among the combined treatments tested (Marostica et al., 2015). The percentages of TGI corroborated the results of RTV. The

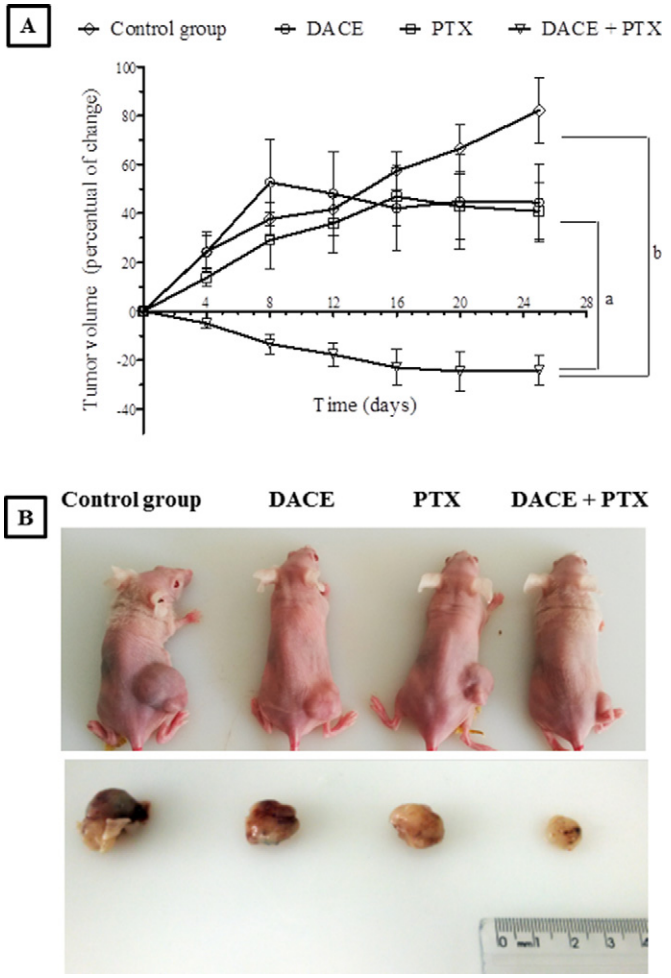

Fig. 1. Results of xenograft lung tumor volume progression measured during and after the treatment protocol. (A) Animals received intravenously the vehicle (control group), DACE 1 mg/kg, PTX 10 mg/kg, and DACE 1 mg/kg + PTX 10 mg/kg. Tumor volume measurements were obtained with a caliper. The data were expressed as mean ± SE of increase or reduction of tumor volume, compared to time zero measurement for each group before treatment ($n = 6$ animals/group). Symbols designate statistical significant differences (one-way ANOVA followed by Tukey's t-test) between indicated treatments. [a]Represent statistical significant differences (p ˜ 0.05) when compared the combined treatment and DACE or PTX individually; [b]Represent statistical significant differences (p ˜ 0.05) when compared the combined treatment and control group. (B) Four days after the last dose applied during each treatment regimen, representative images of animals from each experimental group were obtained as well as representative photographs of tumors removed after euthanasia of animals.

combined treatment inhibited tumor growth by 59.5%, and was more effective than the individual treatments with DACE (20.9%) and PTX (27.5%). Therefore, these *in vivo* results confirmed the synergistic effects already detected *in vitro* (Marostica et al., 2015).

Comparing the changes in the tumor volume during the different days of the experimental protocol (Fig. 1A), it was possible to observe and confirm the data showed in Table 1. Comparing the initial and final time of the treatment with vehicle (control group), the mean tumor volume increased 82.1%. With DACE, the increase of the tumor volume was 44.5%, while with PTX the tumor volume increased 40.9%. Unlike these treatments, the combined therapy with DACE + PTX significantly reduced the average tumor volume by 24.2%. Mice treated with DACE individually showed an increase of tumor volume until day 8 followed by a slight reduction on days 12 and 16, and maintained the tumor volume until the end of the experiment. Mice treated with PTX alone showed an increase of tumor volume until day 16, and maintained the same tumor volume until day 25. With the combined treatment, the tumor volume was reduced until day 16, and maintained this reduction until the end (day 25). The representative images of animals and their respective xenografts lung tumors at the end of the treatments illustrates the data presented, which are novel and highlight the important antitumor activity of the combined therapy with DACE + PTX (Fig. 1B). Furthermore, the antitumor activity of the individual treatments can be compared with previous published data. Another research group (Kausar et al., 2013), using a xenograft model of NSCLC (H1299 cells) and a treatment scheme with cucurbitacin B (1 mg/kg), administered on alternate days for 5 weeks, reported a 70% reduction of the tumor volume, when compared to the untreated control group. Milanovic et al. (2012) demonstrated in a xenograft model of glioblastoma that the single treatment with PTX (10 mg/kg), every three days for fifteen days, showed a tumor growth ratio similar to that of the control group (weights of the excised tumors: 651 ± 148 mg and 764 ± 168 mg, respectively). However, when the combination of PTX with Vadimezan® (5,6-dimethylxanthenone 4-acetic acid derivative, DMXAA) was administered, the tumor growth was completely inhibited (weight of the tumor: 180 ± 56 mg). Wakimoto et al. (2008), using a xenograft model of breast tumor and a treatment regimen with cucurbitacin B (1 mg/kg), three times a week for six weeks, described a tumor volume reduction of 55%, when compared to the untreated mice. Liu et al. (2010), evaluating a xenograft model of laryngeal tumor and a treatment protocol with cucurbitacin B (55 μg/kg), daily for 14 days, detected a tumor volume increase of 1.5-fold, when compared to the beginning of the treatment, but the tumor growth was completely inhibited when a combined treatment with cisplatin (10 mg/kg) and cucurbitacin B was administered. Iwanski et al. (2010) showed in a xenograft model of pancreatic tumor that the treatment with cucurbitacin B (0.5 and 1 mg/kg), three times a week, reduced tumor growth by 18 and 63%, respectively. Nevertheless, when cucurbitacin B was administered (1 mg/kg) combined with gemcitabine (25 mg/kg), the inhibition of tumor growth increased to 83%. A study published by Aribi et al. (2013) using an orthotopic xenograft model of breast cancer and a treatment with cucurbitacin B (0.5 and 1 mg/kg), three times a week, reported a tumor volume reduction, respectively, by 45% and 55%. However, a tumor volume reduction of 90% was detected when the animals received a combined treatment with docetaxel and cucurbitacin B.

Therefore, these results as well as those observed in the present study demonstrated that the combined treatment regimens of cucurbitacin B or it's derivative with anticancer drugs showed a higher therapeutic efficacy, when compared to the individual treatments, highlighting the importance and the need to explore different and novel combination schemes of chemotherapy.

The reduction of TV is a predictive information that is applied for antitumor activity measurement in animal models. However, it is not considered an accurate indicator of antitumor efficacy. After chemotherapy, it is usual the appearance of non-active tissues in tumors, such as apoptotic, fibrotic and necrotic tissues, which make up the residual tumor mass after treatment. Therefore, the measurements of the tumors volume at the end of the experimental protocols usually used to detect antitumor treatments did not reflect accurately the residual disease state (Kubota, 2001). In this perspective, radionuclide scintigraphic images become an important tool along with the measurement data of tumor volume, and can demonstrate the antitumor efficacy due to the labeling of only viable tumoral cells. Due to this fact, in the present study, scintigraphic images of the target area (tumor) and non-target (muscle contralateral) were obtained using the radiotracer ^{99m}Tc-HYNIC-βAla-Bombesin$_{(7-14)}$ (Fig. 2A). Moreover, it was also possible to measure initial and final target to non-target ratios (Fig. 2B) to evaluate the residual viable tumor mass (RVTM) for each treatment. As shown in Fig. 2B, the results of the initial and final target to non-target ratios obtained for the control group, DACE (1 mg/kg), PTX (10 mg/kg) and DACE + PTX were 3.23 ± 0.37; 2.18 ± 0.29; 1.73 ± 0.38 and 0.93 ± 0.14, respectively. When compared with the control group, the treatments with DACE, PTX and DACE + PTX showed a RVTM reduction of 32.5%; 46.4% and 71.2%, respectively. As already presented and discussed concerning tumor volume, RTV and TGI, the combined therapy was also more effective to reduce RVTM. The most effective reduction of RVTM showed by the combined treatment in comparison with the individual treatments suggest that this treatment regimen is less susceptible to the resistance development of NSCLC tumor cells, exactly one of the main purposes of combined treatment schemes in clinical oncology (Chou, 2006; Custodio et al., 2012; Koh et al., 2012). In our previous study, the clonogenic assay showed that the combined treatment of DACE + PTX completely reduced the survival and proliferation rate of A549 cells after treatment withdrawal, which is the same cell line applied to induce xenograft model of NSCLC (Marostica et al., 2015). Therefore, the RVTM data obtained *in vivo* corroborates our previous results obtained *in vitro*. Together, these important insights prove that the combined treatment is less susceptible to NSCLC resistance, which is a main characteristic that unfortunately limits the effectiveness of different treatments of NSCLC. The results concerning RVTM also corroborate and reproduce the synergistic effects obtained *in vitro* with DACE + PTX on A549 cells. In this work, we demonstrated that the synergistic effects of this combined therapy were due to the G2/M cell cycle arrest, cell proliferation pathway modulation, such as Akt and STAT3, increased expression of p53, survivin expression reduction, actin cytoskeletal morphological changes, and cell death by apoptosis by nuclear fragmentation and caspase-dependent manner. Furthermore, it was observed that the combined treatment increased E-cadherin expression and reduced p-cofilin1 and the metalloproteinases expression, especially MMP-2. The antiproliferative effects of DACE associated with PTX were also stimulated by the oxidant agent L-buthionine-sulfoximine, and attenuated by *N*-acetilcysteine, an antioxidant agent, indicating that the possible antiproliferative effect is associated with the generation of reactive oxygen species (Marostica et al., 2015). Moreover, our research group (Silva et al., 2015) using a transgenic mouse model of c-RAF-induced lung adenoma (c-RAF-1-BxB mice) reported that DACE modulated the EGFR-regulated cell proliferation pathway related to dysregulated cell proliferation, resistance and tumor progression in NSCLC. Thus, metastasis modulation could be another effect that may help explain the high antitumor activity detected in this xenograft model of NSCLC.

Another possibility that may explain the detected antitumor efficacy of DACE + PTX combination is related to P-glycoprotein (P-gp) efflux. It is well known that PTX is a substrate to drug efflux in this process (Jang and Au, 2001). Resistant tumors usually overexpress genes related with chemoresistance. These genes encode P-gp synthesis and induce a high efflux of drugs into the extracellular medium, promoting the development of acquired resistance to chemotherapy (Callaghan et al., 2014). Furthermore, it is also known that cucurbitacins, including cucurbitacin B that is the precursor of DACE have been described as efflux inhibitors

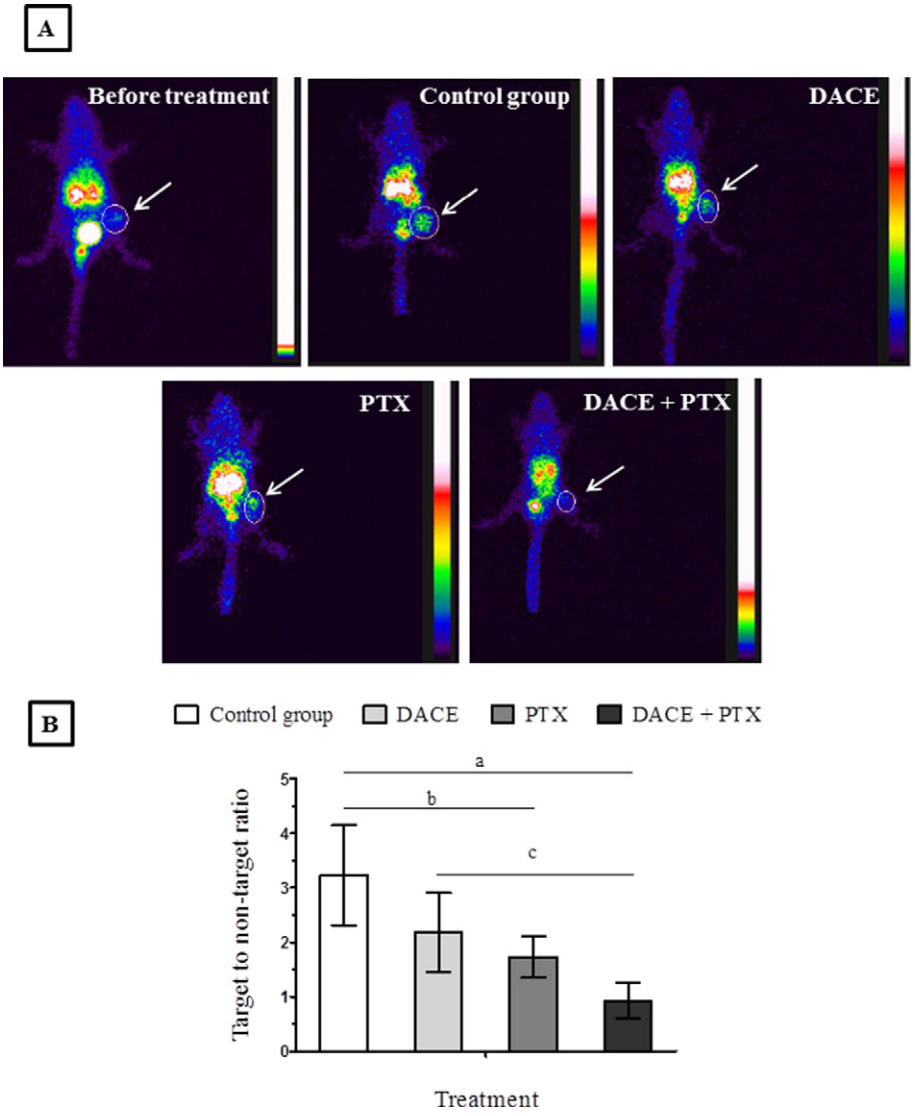

Fig. 2. Scintigraphic images of xenograft lung tumor and target to non-target ratios before and after treatments. (A) Scintigraphic images obtained four hours after intravenous administration of the radioisotope ^{99m}Tc-HYNIC-βAla-Bombesin$_{(7-14)}$, before the administration of the first dose and after six doses of the treatments. The area delineated in red indicates the target area (tumor). Each image represents time zero for all groups (before treatment); and after treatments with vehicle (control group); DACE 1 mg/kg; PTX 10 mg/kg; DACE 1 mg/kg + PTX 10 mg/kg. (B) Target to non-target ratios obtained before (day zero) and after treatments (day 25). Using these scintigraphic images, the relative ratios of target to non-target (initial and after treatments) were calculated considering the target area of the tumor and no target area of the contralateral muscle. Data were expressed as mean ± SE ($n = 6$ animals/group). Symbols indicate statistical significant differences between indicated treatments (one-way ANOVA followed by Tukey's test). [a]Represent statistical significant differences ($p < 0.001$) when compared the combined treatment and control group; [b]Represent statistical significant differences ($p < 0.05$) when compared the PTX treatment and control group. [c]Represent statistical significant differences ($p < 0.001$) when compared combined treatment and DACE alone. (For interpretation of the references to colour in this figure legend, the reader is referred to the web version of this article.)

mediated by P-gp. This characteristic could be also responsible for the promising antitumor synergism showed by cucurbitacins combined with different anticancer drugs (Ramalhete et al., 2009; Abdallah et al., 2015; Sun et al., 2015).

The body weight variation is an important indicator of toxicity after drug treatments, and therefore is one of the parameters that must be monitored during *in vivo* preclinical studies. Fig. 3A shows that no significant body weight changes were detected for all treatment groups. Furthermore, the animals maintained the initial body weight until the end of the treatments and no death was recorded. In addition, histological analyses were performed with different organs at the end of the treatment period, and this evaluation revealed no evidence of toxicity in the brain, heart, lung and spleen of the animals of all treatment groups (data not shown). However, liver tissue showed histological changes suggestive of toxicity, mainly for the animals treated with PTX (10 mg/kg) (Fig. 3B). In these images, it can be observed that the liver tissue of mice from the control and DACE treated groups did not present histological alterations. Unlike this, the liver tissue of animals that received PTX showed histological changes classified as severe hydropic degeneration, while animals treated with DACE + PTX also showed hydropic degeneration of hepatocytes, but classified as discrete. The hydropic degeneration of hepatocytes, also described as cellular edema or cytosol swelling, is a non-lethal cell injury process characterized by water accumulation in the cytosol due to the impairment of the Na^+/K^+ ATPase pump. It is a reversible process, and when the injurious agent is removed, cells can assume their normal function, usually with no functional impairment to organ or tissue (Jarrar and Taib, 2012). These histological data also confirm the hypothesis of our study. As described, the combined treatment has shown the most effective

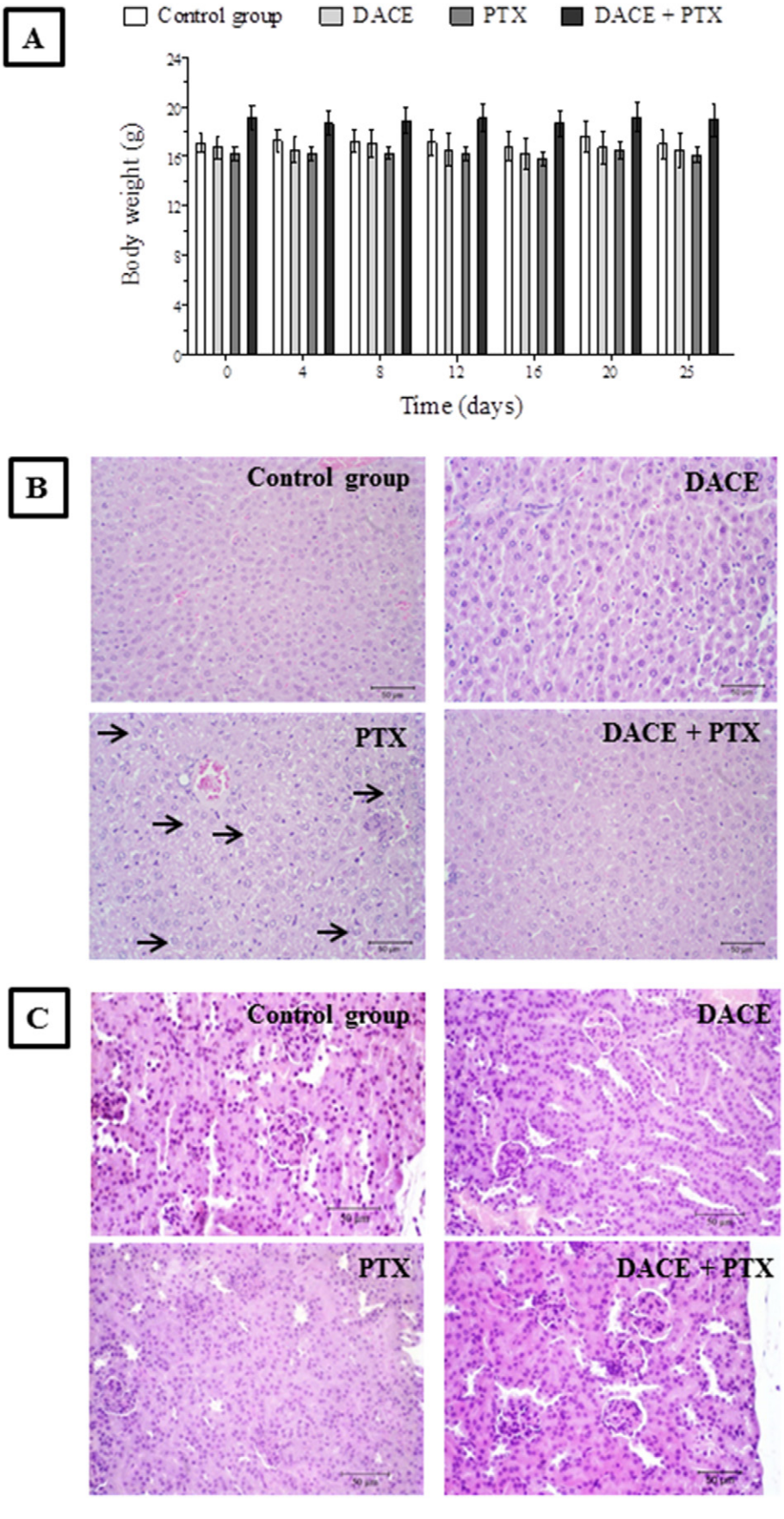
A
Control group
DACE
PTX
DACE + PTX
Body weight (g)
Time (days)
B
Control group
DACE
PTX
DACE + PTX
C
Control group
DACE
PTX
DACE + PTX

Table 2
Biochemical markers of liver and kidney function of mice that received the different treatments.

Biochemical markers	Control group	DACE 1 mg/kg	PTX 10 mg/kg	DACE 1 mg/kg + PTX 10 mg/kg
Albumin (mg/dL)	2.15 ± 0.14	1.98 ± 0.11	2.22 ± 0.16	2.18 ± 0.15
Total protein (mg/dL)	3.00 ± 0.13	3.02 ± 0.13	3.41 ± 0.20	2.82 ± 0.13
Alkaline phosphatase (U/L)	61.80 ± 8.15	68.10 ± 12.12	67.30 ± 13.30	58.10 ± 7.80
AST (U/L)	82.5 ± 9.93	95.4 ± 17.8[a]	78.2 ± 8.32	49.1 ± 4.40[d]
ALT (U/L)	13.1 ± 2.00	24.6 ± 5.10[b]	20.6 ± 2.86[c]	14.1 ± 2.60
Urea (mg/dL)	48.70 ± 2.50	50.20 ± 13.90	60.80 ± 2.80	62 ± 6.75

Data represent the mean ± SE ($n = 6$ animals/group). Symbols indicate statistical significant differences (one-way ANOVA followed by Tukey's test) comparing different treatments.
[a] Represent statistical significant differences ($p < 0.05$) for AST levels when compared the DACE alone treatment and control group.
[b] Represent statistical significant differences ($p < 0.05$) for ALT levels when compared DACE alone treatment and control group.
[c] Represent statistical significant differences ($p < 0.05$) for ALT levels when compared the PTX alone treatment and control group.
[d] Represent statistical significant differences ($p < 0.05$) for AST levels when compared the combined treatment and control group.

antitumor activity and showed discrete hepatocytes histological alterations when compared to the treatment with PTX alone, which was classified as severe. The treatment with DACE individually did not induce hepatocyte degeneration. Regarding to nephrotoxicity, no histological changes were detected for all mice (Fig. 3C).

Some biochemical parameters of liver and kidney function were also evaluated, and the results are shown in Table 2. All treatment regimens have not significantly altered the levels of albumin, total protein and alkaline phosphatase in comparison with the control group. However, discrete alterations in liver enzymes, such as AST and ALT, were detected. AST activity showed a significant increase after treatment with DACE alone and a significant decrease after the combined treatment. ALT activity showed a significant increase with DACE and PTX treatments individually, and stayed in with the combined treatment. These results partially corroborate those published by Mandaliya et al. (2015), who reported that the combined treatment of PTX with trastuzumab, administered to a patient with breast cancer, initially induced a slight increase in the activity of ALT and AST with subsequent induction of acute hepatic necrosis, which was detected only after the death of this patient. Despite this, in the present study, we did not observe histological changes related to acute hepatic necrosis in the liver tissue of the animals. Regarding to urea serum concentration, a marker of kidney function, we did not detect significant changes among the different treatments, which can indicate that no treatment regimen impaired kidney function. These data also corroborate the histological images of kidney tissue after treatments (Fig. 3C). Therefore, no treatment regimen induced histological and biochemical changes indicative of nephrotoxicity.

Immunohistochemically, all xenograft tumor tissues exhibited positive nuclear staining for Ki67, a cell proliferation marker, indicating that xenograft tissues were obtained from actively proliferative tumors (Fig. 4). Reduced cellularity and visually a lower number of Ki67 positive cells were observed in tumors xenografts of animals that received combined therapy (1%–8% of stained tumor cells, Fig. 4D), when compared to tumor xenografts of mice receiving treatments with DACE and PTX alone (12%–27%, Fig. 4B and Fig. 4C, respectively) or the control group (51%–92% of stained tumor cells, Fig. 4A). Overall, this evidence suggests that the treatments and especially the combined therapy were more effective to inhibit cell proliferation and NSCLC progression. Such behavior is expected since the histological analysis of tumors showed an increasement in cell apoptosis and a more expressive tumor volume reduction following the combined treatment.

4. Conclusion

The obtained data indicate that the combined therapy (DACE + PTX) was more effective to reduce growth and tumor volume, when compared with individual treatments and untreated group. Xenograft lung tumors of animals that received the combined therapy also showed the greatest reduction of residual viable tumor mass since it was more effective to inhibit cell proliferation, which may suggest that this treatment scheme was less susceptible to induce drug resistance. All treatments were well tolerated by the animals and no significant body weight changes were detected. Furthermore, the combined treatment did not induce damage compatible with hepatotoxicity and nephrotoxicity according to the histological and biochemical markers evaluated. To our knowledge, this is the first report of this combined treatment in a xenograft model of NSCLC. Taken together, these insights show that this combined therapy presented promising antitumor activity *in vivo* with no toxicity to non-tumor tissues, and the development of resistance to the combined treatment against NSCLC was less likely to occur.

Ethical approval

All *in vivo* procedures performed in this study were approved by the Committee on Care and Use of Experimental Animal Resources from the *Universidade Federal de Minas Gerais* (protocol number 118/2015).

Author contributions

All authors made substantial contributions to design, acquisition of data, analyses and interpretation of the data, as well as in drafting the article or revising it critically for important intellectual content. All authors read and approved the final draft of the manuscript.

Fig. 3. Body weight measurements, and liver and kidney tissues of BALB/c nude mice with NSCLC xenograft tumor after the administration of different treatments. (A) The body weight of animals was measured every four days, after each dose administered. No statistical significant differences were detected (one-way ANOVA followed by Tukey's test), and data were expressed as mean ± SE ($n = 6$ animals/group). (B) (C) Photomicrographs representative of histological preparations stained with hematoxylin-eosin solution to liver (B) and kidney (C) tissues after intravenous administration of vehicle (control group), DACE 1 mg/kg, PTX 10 mg/kg, and DACE 1 mg/kg + PTX 10 mg/kg. Black arrows indicate cells with hydropic degeneration. Scale bars: 50 um; magnification 400×.

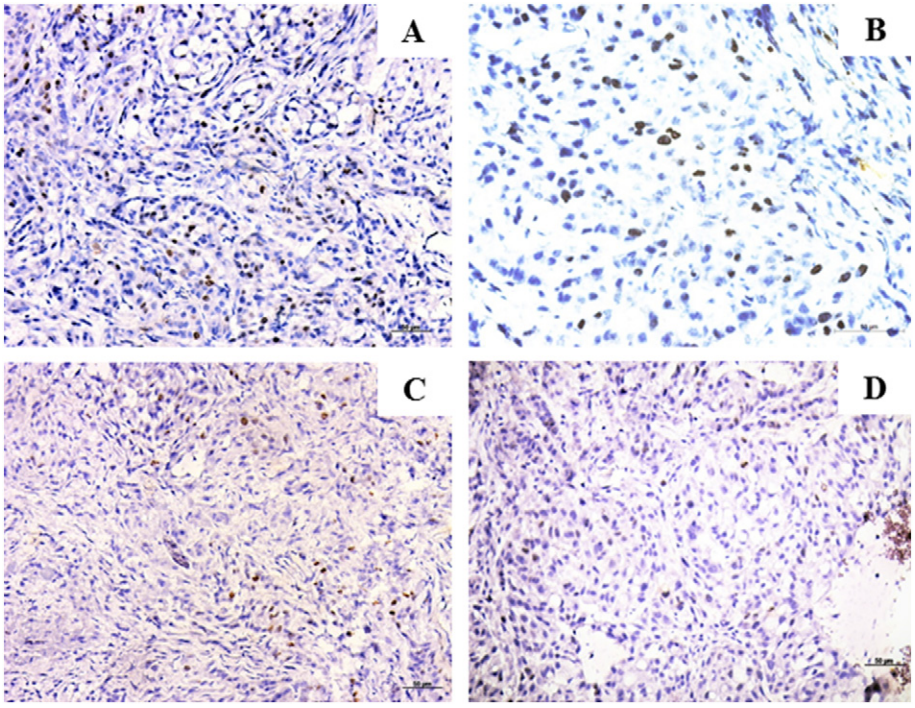

Fig. 4. Immunohistochemistry of NSCLC xenograft tumors stained with the cancer cell proliferation biomarker Ki67, after the administration of different treatments. (A) Control group (vehicle) revealing intense positive nuclear staining (51 to 92% of stained tumor cells); (B) Tumor xenograft tissue from DACE treated group revealing moderate cell proliferation ratio (12 to 27%); (C) Tumor xenograft tissue from PTX treated group revealing low to moderate cell proliferation ratio (12 to 27%); (D) Tumor xenograft tissue from DACE + PTX treated group revealing rare Ki67 stained cells (1 to 8%). DAB immunohistochemistry (blue). Harris hematoxylin counterstained (nuclear staining/purple and cytosolic staining/pink). Brown stain of the nuclei indicate cells positive for the antigen ki67. Scale bars: 50 um; magnification 400×. (For interpretation of the references to colour in this figure legend, the reader is referred to the web version of this article.)

Funding

The authors acknowledge the financial support of *Fundação de Apoio à Pesquisa Científica e Tecnológica do Estado de Santa Catarina*, FAPESC, SC, and *Fundação de Amparo à Pesquisa do Estado de Minas Gerais*, FAPEMIG, MG (grants 56795/2010 and Rede-40/11-PPM-00477-13, respectively) as well as CNPq (MCTI, grants 472979/2011-6 and 408496/2013-4, the later for the acquisition of the nude mice). The authors also thank CAPES (MEC) and CNPq for their research fellowships.

Conflict of interest

The authors declare no conflicts of interest.

References

Abdallah, H.M., Al-Abd, A.M., El-Dine, R.S., El-Halawani, A.M., 2015. P-glycoprotein inhibitors of natural origin as potential tumor chemo-sensitizers: a review. J. Adv. Res. 6, 45–62.

Alghasham, A.A., 2013. Cucurbitacins – a promising target for cancer therapy. Int. J. Health Sci. 7, 77–89.

Ansari, J., Shackelford, R.E., El-Osta, H., 2016. Epigenetics in non-small cell lung cancer: from basics to therapeutics. Transl. Lung Cancer Res. 5, 155–171.

Aribi, A., Gery, S., Lee, D.H., Thoennissen, N.H., Thoennissen, G.B., Alvarez, R., Ho, Q., Lee, K., Doan, N.B., Chan, K.T., Toh, M., Said, J.W., Koeffler, H.P., 2013. The triterpenoid cucurbitacin B augments the antiproliferative activity of chemotherapy in human breast cancer. Int. J. Cancer 132, 2730–2737.

Arumuggam, N., Bhowmick, N.A., Rupasinghe, H.V.P., 2015. A review: phytochemicals targeting JAK/STAT signaling and IDO expression in cancer. Phytother. Res. 29, 805–817.

Cai, Y., Fang, X., He, C., Li, P., Xiao, F., Wang, Y., Chen, M., 2015. Cucurbitacins: a systematic review of the phytochemistry and anticancer activity. Am. J. Chin. Med. 43, 1331–1350.

Callaghan, R., Luk, F., Bebawy, M., 2014. Inhibition of the multidrug resistance P-glycoprotein: time for a change of strategy? Drug Metab. Dispos. 42, 623–631.

Chen, J.C., Chiu, M.H., Nie, R.L., Cordell, G.A., Qiu, S.X., 2005. Cucurbitacins and cucurbitane glycosides: structures and biological activities. Nat. Prod. Rep. 22, 386–399.

Chen, X., Bao, J., Guo, J., Ding, Q., Lu, J., Huang, M., Wang, Y., 2012. Biological activities and potential molecular targets of cucurbitacins: a focus on cancer. Anti-Cancer Drugs 23, 777–787.

Chen, Z., Fillmore, C.M., Hammerman, P.S., Kim, C.F., Wong, K.-K., 2014. Non-small cell lung cancers: a heterogeneous set of diseases. Nat. Rev. Cancer 14, 535–546.

Chou, T.C., 2006. Theoretical basis, experimental design, and computerized simulation of synergism and antagonism in drug combination studies. Pharmacol. Rev. 58, 621–681.

Custodio, A., Méndez, M., Provencio, M., 2012. Targeted therapies for advanced non-small-cell lung cancer: current status and future implications. Cancer Treat. Rev. 38, 36–53.

De Barros, A.L.B., Mota, L.G., Soares, D.C.F., Coelho, M.M.A., Oliveira, M.C., Cardoso, V.N., 2011. Tumor bombesin analog loaded long-circulating and pH-sensitive liposomes as tool for tumor identification. Bioorg. Med. Chem. Lett. 21, 7373–7375.

De Barros, A.L.B., Mota, L.G., Ferreira, C.A., Corrêa, N.C.R., De Goés, A.M., Oliveira, M.C., Cardoso, V.N., 2013. ^{99m}Tc-labeled bombesin analog for breast cancer identification. J. Radioanal. Nucl. Chem. 295, 2083–2090.

Devarakonda, S., Morgensztern, D., Govindan, R., 2015. Genomic alterations in lung adenocarcinoma. Lancet Oncol. 16, 342–351.

Diniz, S.O., Rezende, S.M., Serakides, R., Ferreira, R.L., Ribeiro, T.G., Martin-Comin, J., Cardoso, V.N., 2008. Scintigraphic imaging using technetium-99m-labeled ceftizoxime in an experimental model of acute osteomyelitis in rats. Nucl. Med. Commun. 29, 830–836.

Huang, G.S., Lopez-Barcons, L., Freeze, B.S., Smith, A.B., Goldberg, G.L., Horwitz, S.B., McDaid, H.M., 2006. Potentiation of taxol efficacy by discodermolide in ovarian carcinoma xenograft-bearing mice. Clin. Cancer Res. 12, 298–304.

Iwanski, G.B., Lee, D.H., En-gal, S., Doan, N.B., Castor, B., Vogt, M., Toh, M., Bokemeyer, C., Said, J.W., Thoennissen, N.H., Koeffler, H.P., 2010. Cucurbitacin B, a novel in vivo potentiator of gemcitabine with low toxicity in the treatment of pancreatic cancer. Br. J. Pharmacol. 160, 998–1007.

Jang, S.H., Wientjes, M.G., Au, J.L., 2001. Kinetics of P-glycoprotein-mediated efflux of paclitaxel. J. Pharmacol. Exp. Ther. 298, 1236–1242.

Jarrar, B.M., Taib, N.T., 2012. Histological and histochemical alterations in the liver induced by lead chronic toxicity. Saudi J. Biol. Sci. 19, 203–210.

Kausar, H., Munagala, R., Bansal, S.S., Agil, F., Vadhanam, M.V., Gupta, R.C., 2013. Cucurbitacin B potently suppresses non-small-cell lung cancer growth: identification of intracellular thiols as critical targets. Cancer Lett. 332, 35–45.

Kaushik, U., Aeri, V., Mir, S.R., 2015. Cucurbitacins – an insight into medicinal leads from nature. Pharmacogn. Rev. 9, 12–18.

Koh, P.K., Faivre-Finn, C., Blackhall, F.H., De Ruysscher, D., 2012. Targeted agents in non-small cell lung cancer (NSCLC): clinical developments and rationale for the combination with thoracic radiotherapy. Cancer Treat. Rev. 38, 626–640.

Kubota, K., 2001. From tumor biology to clinical PET: a review of positron emission tomography (PET) in oncology. Ann. Nucl. Med. 15, 471–486.

Lang, K.L., Guimarães, T., Machado, V.R., Zimmermann, L., Silva, I.T., Teixeira, M.R., Durán, F.J., Palermo, J.A., Simões, C.M.O., Caro, M.B.C., Schenkel, E.P., 2011. New cytotoxic cucurbutacins from *Wilbrandia ebracteata* Cogn. Planta Med. 77, 1648–1651.

Lang, K.L., Silva, I.T., Zimmermann, L., Machado, V.R., Teixeira, M.R., Lapuh, M.I., Galleti, M.A., Palermo, J.A., Cabrera, G.M., Bernardes, L.S.C., Simões, C.M.O., Schenkel, E.P., Caro, M.S.B., Durán, F.J., 2012. Synthesis and cytotoxic activity evaluation of dihydrocucurbitacin B and cucurbitacin B derivatives. Bioorg. Med. Chem. 20, 3016–3030.

Lang, K.L., Silva, I.T., Machado, V.R., Zimmermann, L., Caro, M.S.B., Simões, C.M.O., Schenkel, E.P., Durán, F.J., Bernardes, L.S.C., Melo, E.B., 2014. Multivariate SAR and QSAR of cucurbitacin derivatives as cytotoxic compounds in a human lung adenocarcinoma cell line. J. Mol. Graph. Model. 48, 70–79.

Lee, D.H., Iwanski, G.B., Thoennissen, N.H., 2010. Cucurbitacin: ancient compound shedding new light on cancer treatment. Sci. World J. 10, 413–418.

Li, F., Zhao, C., Wang, L., 2014. Molecular-targeted agents combination therapy for cancer: developments and potential. Int. J. Cancer 134, 1257–1269.

Liu, T., Peng, H., Zhang, M., Deng, Y., Wu, Z., 2010. Cucurbitacin B, a small molecule inhibitor of the Stat3 signaling pathway, enhances the chemosensitivity of laryngeal squamous cell carcinoma cells to cisplatin. Eur. J. Pharmacol. 641, 15–22.

Mandaliya, H., Baghi, P., Prawira, A., George, M.K., 2015. A rare case of paclitaxel and/or trastuzumab induced acute hepatic necrosis. Case Rep. Oncol. Med. 2015, 1–2.

Marostica, L.L., Silva, I.T., Kratz, J.M., Persich, L., Geller, F.C., Lang, K.L., Caro, M.S., Durán, F.J., Schenkel, E.P., Simões, C.M.O., 2015. Synergistic antiproliferative effects of a new cucurbitacin B derivative and chemotherapy drugs on lung cancer cell line A549. Chem. Res. Toxicol. 28, 1949–1960.

Marostica, L.L., De Barros, A.L.B., Silva, J.O., Lopes, S.C., Salgado, B.S., Chondrogiannis, S., Rubello, D., Cassali, G.D., Schenkel, E.P., Cardoso, V.N., Simões, C.M.O., Oliveira, M.C., 2016. Feasibility study with 99m Tc-HYNIC-β-Ala-Bombesin$_{(7-14)}$ as an agent to early visualization of lung tumor cells in nude mice. Nucl. Med. Commun. 37, 372–376.

Milanovic, D., Braun, F., Weber, W., Grosu, A.L., Behe, M., Niedermann, G., 2012. The influence of the combined treatment with vadimezan (ASA404) and taxol on the growth of U251 glioblastoma xenografts. BMC Cancer 12, 1–8.

Newman, D.J., Cragg, G.M., 2016. Natural products as sources of new drugs from 1981 to 2014. J. Nat. Prod. 79, 629–661.

Ramalhete, C., Molnár, J., Mulhovo, S., Rosário, V.E., Ferreira, M.J., 2009. New potent P-glycoprotein modulators with the cucurbitane scaffold and their synergistic interaction with doxorubicin on resistant cancer cells. Bioorg. Med. Chem. 17, 6942–6951.

Ríos, I., Andújar, J.M., Escandell, R.M., Recio, M.C., 2012. Cucurbitacins as inducers of cell death and a rich source of potential cancer compounds. Curr. Pharm. Design 18, 1663–1676.

Roland, C.L., Dineen, S.P., Lynn, K.D., Sullivan, L.A., Dellinger, M.T., Sadegh, L., Sullivan, J.P., Shames, D.S., Brekken, R.A., 2009. Inhibition of vascular endothelial growth factor reduces angiogenesis and modulates immune cell infiltration of orthotopic breast cancer xenografts. Mol. Cancer Ther. 8, 1761–1771.

Siegel, R.L., Miller, K.D., Jemal, A., 2017. Cancer statistics, 2017. CA Cancer J. Clin. 67, 7–30.

Silva, I.T., Teixeira, M.R., Lang, K., Guimarães, T.R., Dudek, S.E., Durán, F.J., Ludwig, S., Caro, M.S.B., Schenkel, E.P., Simões, C.M.O., 2013. Proliferative inhibition and apoptotic mechanism on human non-small-cell lung cancer (A549 cells) of a novel cucurbitacin from *Wilbrandia ebracteata* Cogn. Int. J. Cancer Res. 9, 54–68.

Silva, I.T., Carvalho, A., Lang, K.L., Dudek, S.E., Durán, F.J., Caro, M.S.B., Rapp, U.R., Wixler, V., Schenkel, E.P., Simões, C.M.O., Ludwig, S., 2015. In vitro and in vivo antitumor activity of a novel semisynthetic derivative of cucurbitacin B. PLoS One 10 (2), e0117794.

Sun, Y., Zhang, J., Zhou, J., Huang, Z., Hu, H., Qiao, M., Zhao, X., Chen, D., 2015. Synergistic effect of cucurbitacin B in combination with curcumin *via* enhancing apoptosis induction and reversing multidrug resistance in human hepatoma cells. Eur. J. Pharmacol. 768, 28–40.

Wakimoto, N., Yin, D., O'Kelly, J., Haritunians, T., Karlan, B., Said, J., Xing, H., Koeffler, H.P., 2008. Cucurbitacin B has a potent antiproliferative effect on breast cancer cells in vitro and in vivo. Cancer Sci. 99, 1793–1797.

Wall, M.E., Wani, M.C., 1995. Camptothecin and taxol: discovery to clinic – thirteenth Bruce F. Cain Memorial Award Lecture. Cancer Res. 55, 753–760.

Yamori, T., Sato, S., Chikasawa, H., Kadota, T., 1997. Anti-tumor efficacy of paclitaxel against human lung cancer xenografts. J. Cancer Res. Ther. 88, 1205–1210.